Archives of Hydro-Engineering and Environmental Mechanics
Vol. 53 (2006), No. 1, pp. 71–94

Deformation Measurements in Granular Bodies Using a Particle Image Velocimetry Technique

Cezary Słomiński*, Maciej Niedostatkiewicz, Jacek Tejchman****

* Karlsruhe University, Institute for Soil and Rock Mechanics, Karlsruhe, Germany,
** Gdańsk University of Technology, Faculty of Civil and Environmental Engineering, ul. G. Narutowicza 11/12, 80-952 Gdańsk, Poland, e-mail: tejchmk@pg.gda.pl

(Received October 12, 2005; revised February 07, 2006)

Abstract

The paper presents results of strain measurements in cohesionless sand in two different boundary value problems, namely quasi-static pull-out test of a steel wall and confined granular flow in a rectangular model silo using a non-destructive method called Particle Image Velocimetry (PIV) which is a technique for measuring surface displacements from digital images. Advantages and disadvantages of the method are outlined.

Key words: PIV, pull-out test, sand, silo flow, strain, wall roughness

1. Introduction

Localization of deformation in the form of narrow zones of intense shearing is a fundamental phenomenon in granular materials. Thus, it is of primary importance to take it into account while modeling the behaviour of granulates. Localization under shear occur in the interior domain in either the form of spontaneous shear zones or on interfaces in the form of induced shear zones where structural members interact and stresses are transferred from one member to the other. The localized shear zones inside the material are closely related to its unstable behaviour. Moreover, an understanding of the mechanism of the formation of shear zones is important since they act as a precursor to ultimate soil failure. The knowledge of the deformation field is also important to calibrate constitutive laws describing the behaviour of granular materials.

Different techniques have been used to capture shear zones and other non-homogeneous deformations in granular bodies during laboratory tests: coloured layers and markers (Tejchman 1989, Yoshida et al 1994), X-rays (Roscoe et al 1963, James 1965, Vardoulakis 1977, Michalowski 1984, 1990, Gudehus

1986, Tejchman and Wu 1995), gamma-rays (Tan and Fwa 1991), photogrammetry and stereo-photogrammetry (Butterfield et al 1970, Desrues 1984, Desrues and Viggiani 2004), X-ray-tomography (Mokni 1992, Desrues et al 1996, Baxter and Behringer 1990), electrical tomography (ECT, Jaworski and Dyakowski 2001, Niedostatkiewicz and Tejchman 2005) and Particle Image Velocimetry (PIV, Adrian 1991, Raffel et al 1998, Vacher et al 1999, Lueptov et al 2000, Nübel 2002, Hutter and Kirchner 2003, White et al 2003, Kohse 2003, Fischer et al 2005, Sielamowicz et al 2005, Zadroga i Malesiński 2005). Nowadays, the last non-invasive method has become very popular worldwide. It is a technique for measuring surface displacements on the basis of the analysis of successive pairs of digital photographs of the side of a deforming specimen. It operates by matching pixel gray values between digital images, thus enabling highly accurate displacement measurements.

The intention of the paper is to show the potential of the Particle Image Velocimetry (PIV) technique to measure directly internal displacements in plane strain specimens of cohesionless sand during the pull-out test of a wall and confined granular flow in a model silo. The silo results were compared with results obtained with X-rays (Michalowski 1984, 1990, and Baxter and Behringer 1990). The measurements were carried out in the co-operation of Gdańsk University of Technology with the Karlsruhe University where this method was comprehensively tested, examined with respect to accuracy and used succesfully to identify shear zones during different granular problems (Nübel 2002, Kohse 2003).

2. Particle Image Velocimetry (PIV)

PIV is a powerful optical surface velocity-measuring tool to visualize two-dimensional deformations (Adrian 1991) which was originally developed in the field of experimental fluid and gas mechanics (Raffel et al 1998). In contrast to fluids or gases, it does not need any intrusive markers to be installed in granulates since the grains themselves serve as tracers. Its advantage lies in its simplicity. A high resolution monitoring of different deformations can be obtained by processing successive digital images. Owing to this shear localization can be visualized and analysed in detail (Nübel 2002, Kohse 2003, Rechenmacher and Finno 2004). The PIV system interprets differences in light intensity as a gray-scale pattern recorded at each pixel on CCD-camera (Charge Coupled Device). The camera remains in a fixed position with the camera axis oriented perpendicular to the plane of deformation. Two functions are of major importance for PIV: image field intensity and cross-correlation function (Hutter and Kirchner 2003). The image intensity field assigns to each point in the image plane a scalar value (grey scale pattern in the *.bmp format) which reflects the light intensity of the corresponding point in the physical space (it maps simply the light energy of an individual particle in a physical space into an intensity value in the image plane). The gray levels

range numerically between 0 (black) and 255 (pure white) for an 8-bit image. A deformation pattern is detected by comparing two consecutive images captured by a camera. A so-called area of interest (AOI) is cut out of the digital image and divided into small disjointed sub-areas called interrogation cells (patches) (Fig. 1). Each cell comprises a particular number of digital pixels from 8×8 to 64×64 pixels (square subsets of pixels). If the deformation between two consecutive images is sufficiently small, the patterns of the interrogation cells should not change their characteristics (only their locations). To find a local displacement between images 1 and 2, a search zone is extracted from the second image (Fig. 2). A correct local displacement vector for each interrogation cell is accomplished by means of a cross-correlation function between two consecutive brightness distributions in two digital images (Fig. 3):

$$R(\Delta x, \Delta y) = R(s) = \sum_{x=0,y=0}^{x<n,y<n} I_1(x, y) I_2(x + \Delta x, y + \Delta y), \tag{1}$$

wherein R – quantity of correlation, x and y – coordinates in the image 1, Δx and Δy – displacement increments from image 1 to image 2, I_1 and I_2 – image intensities of the interrogation cell of the consecutive images 1 and 2, and n – size of the interrogation cell, respectively. The correlation plane is evaluated at single pixel intervals. By fitting a bicubic interpolation to the region close to the peak, the displacement vector is established to sub-pixel resolution of 0.005 pixels. The 2D array of the values R gives the correlation values for all displacements $(\Delta x, \Delta y)$ between two interrogation cells. The function calculates simply possible displacements by correlating all gray values from the first image with all gray values from the second image. The peak in the correlation function indicates that the two images overlap each other (this indicates the 'degree of match' between two images), Fig. 3. Thus, the displacement field between the image pair can be constructed (the correlation offset is equal to the displacement vector). Only one displacement vector is calculated within one interrogation cell (this is an average displacement vector of all particles within the interrogation cell). The procedure is continued by substituting the second image with a subsequent image. Thus, the evolution of displacements in the specimen can be captured. The existing errors due to convolution of the mean intensities and fluctuating noise in Fig. 3 can be disregarded. The correlation operation in Eq. 1 is conducted in the frequency domain by taking the fast Fourier transform (FFT) of each patch (instead of numerical operations realized in the time domain). The result of the cross correlation between two images is received as an inverse matrix of FFT. A direct PIV evaluation leads to a Eulerian description with independent coordinates $u_t(x, y)$ (Fig. 4) since the area of interest and the interrogation cell size are fixed. The relative displacements are next converted into a Lagrangian deformation field yielding total deformations with respect to the initial configuration. It is done by

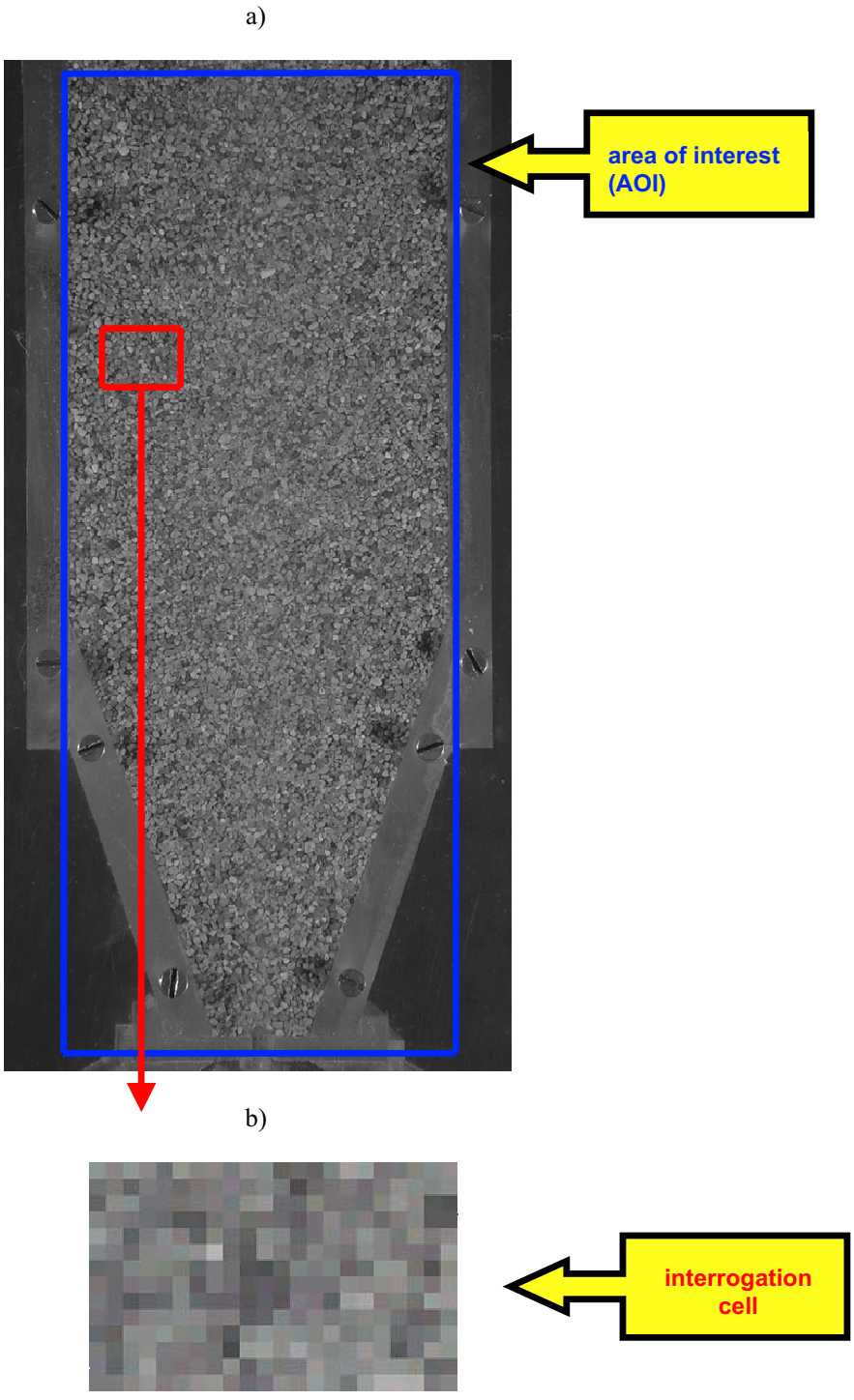

Fig. 1. Digital image for silo flow: a) area of interest (AOI) and b) interrogation cell

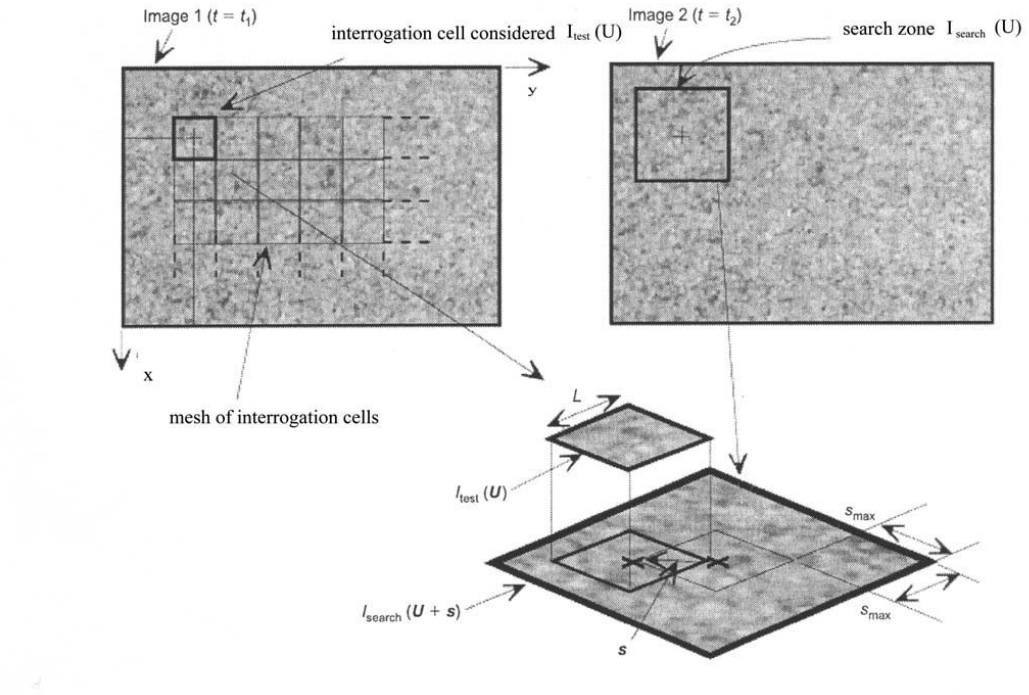

Fig. 2. PIV analysis (White et al 2003) (s – displacement)

means of a linear 2D interpolation (Nübel 2002) where the deformation of a node of the deformed mesh can be calculated as:

$$u(m,n) = \omega_1 u_t(i,j) + \omega_2 u_t(i+1,j) + \omega_3 u_t(i,j+1) + \omega_4 u_t(i+1,j+1). \quad (2)$$

Herein, the factors ω_i are the linear weighting factors depending on the position of nodes $u(m,n)$ in the lattice, and the u_t are the actual relative displacements of the referenced lattice site calculated by Eq. 1. The strain vector $[E] = \{\varepsilon_{11}\varepsilon_{12}\varepsilon_{21}\varepsilon_{22}\}^T$ is calculated with a strain-displacement matrix $[B]$ used in FEM

$$[E] = [B][u], \quad (3)$$

where $[u] = \left(u_1^{(1)}u_2^{(1)}u_1^{(2)}u_2^{(2)}u_1^{(3)}u_2^{(3)}u_1^{(4)}u_2^{(4)}\right)^T$ is the displacement vector. The plane strain 4-node element is described by the following matrix $[B]$:

$$[B] = \begin{bmatrix} N_{,1}^{(1)} & 0 & N_{,1}^{(2)} & 0 & N_{,1}^{(3)} & 0 & N_{,1}^{(4)} & 0 \\ 0 & N_{,2}^{(1)} & 0 & N_{,2}^{(2)} & 0 & N_{,2}^{(3)} & 0 & N_{,2}^{(4)} \\ N_{,2}^{(1)} & N_{,1}^{(1)} & N_{,2}^{(2)} & N_{,1}^{(2)} & N_{,2}^{(3)} & N_{,1}^{(3)} & N_{,2}^{(4)} & N_{,1}^{(4)} \end{bmatrix}, \quad (4)$$

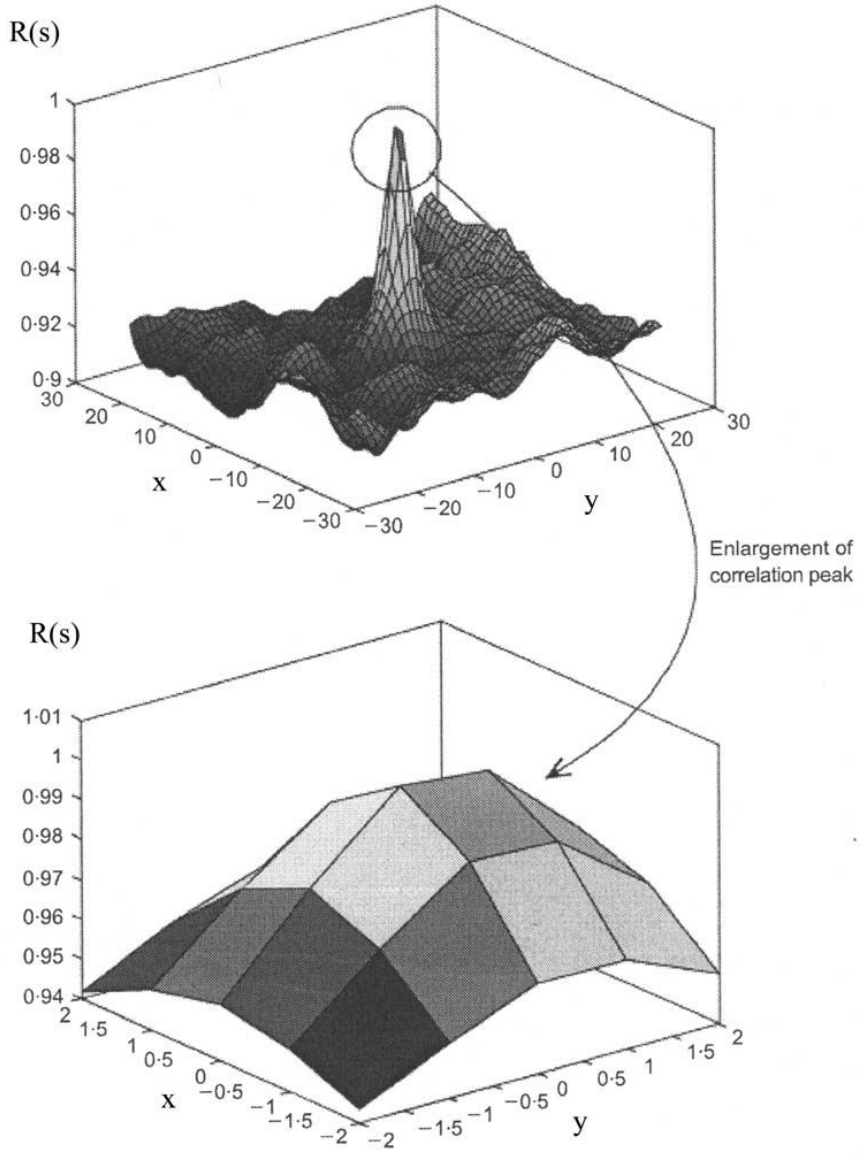

Fig. 3. Correlation plane with correlation peak (White et al 2003)

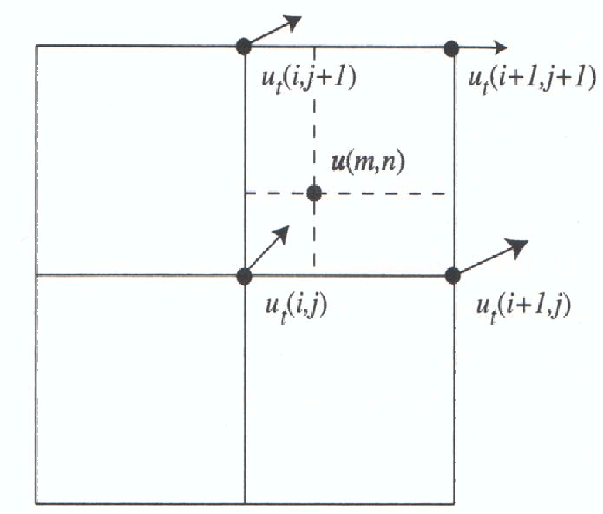

Fig. 4. Transformation from Euler to Lagrangian coordinates (Nübel 2002)

where $N,_j^{(i)}$ is the partial derivative of the shape function associated with the node i with respect to x_j.

In order to eliminate high frequency noise, a smoothing filter is applied to each vector field by taking an average value of the neighborhood of pixels (Nübel 2002). A filter calculates a new grey value of each pixel by laying a special filter mesh on the mesh of initial pixels (the values of initial pixels are multiplied with the values of the filter mesh and then added to each other). The type of the filter insignificantly influences the thickness of the shear zone (Kohse 2003).

The PIV-photogrammetry system has a measured precision of $1/15000^{th}$ of the field of view (White et al 2003). The accuracy of the measured displacements in the deforming specimen during a quasi-static plane strain compression test was found to be less than 0.01 mm (Rechenmacher and Finno 2004, Bhandari and Inoue 2005).

The disadvantages of the PIV method are that strains inside the material cannot be traced (only those on the surface of the specimen) and the size of the plane specimen cannot be large.

The PIV technique is subject to certain errors as: image distortion from the medium between the camera lens and the specimen (non-coplanarity of the camera and object plane, radial and tangential lens distortion), refraction through a viewing window, pixel non-squareness (White et al 2003) and boundary effects (Hutter and Kirchner 2003). These errors have a rather negligible effect on the determined displacements, as each successive photograph is affected equally by these inaccuracies. The measurement accuracy depends on the test patch size. The larger the patch size, the smaller the scatter. A conservative estimate of random errors can be expressed by the following equation (White et al 2003):

$$\rho_{pixel} = \frac{0.6}{L} + \frac{150000}{L^8}, \tag{5}$$

where L is the patch size. The patch of 16×16 pixels was found to be distributed around zero mean with a standard error of 0.005 pixels, and the patch of 50×50 pixels with a standard error of 0.0007 pixels (White et al 2003). However, the smaller the patch, the greater number of measurement points. Due to the fact that the photographs are large (e.g. 51×38 cm^2) and the image resolution is high (e.g. 2272×1704 or 2560×1920 – i.e. significantly higher than 640×480), the effect of the image compression (intensity reduction) is insignificant.

The whole procedure can be summarised as follows (Nübel 2002, White et al 2003, Hutter and Kirchner 2003):

- subdivide the image into interrogation cells,
- calculate the image intensity fields at time t and $t + \Delta t$ for one interrogation cell,
- calculate the correlation between image intensity fields (the most likely displacement is the peak of the function),
- repeat the procedure for each interrogation cell,
- convert the Eulerian deformation field into Lagrangian deformation field,
- calculate strain tensor.

For further details of the technique regarding the underlying principle, accuracy and performance, the reader is referred to (Adrian 1991, Raffel et al 1998, Sutton et al 2000, Nübel 2002, White et al 2003, and Hutter and Kirchner 2003). A detailed description of the programme used in the PIV technique can be found in the work by Kohse (2003).

3. Experimental Results

3.1. Quasi-Static Pull-Out Test

In the test, a rigid metal wall was vertically pulled out from a granular material. A test was carried out to approximately model the two-dimensional interface behaviour between soil and structure. The tests were carried out with so-called Karlsruhe sand (mean grain diameter $d_{50} = 0.5$ mm, uniformity coefficient $U = 2$). The glass container with a sand specimen had the following dimensions: length 0.5 m, width 0.25 m and height 0.2 m (Fig. 5). The metal wall with a height of 0.2 m (placed at the container wall) was smooth, rough and very rough. A teflon layer was used to reduce the friction between the metal wall and container. A smooth metal wall was bare steel plate, a rough one had a coat of so-called Stuttgart sand (mean grain diameter $d_{50} = 0.2$ mm) and a very rough wall was obtained by gluing Karlsruhe sand to the wall surface.

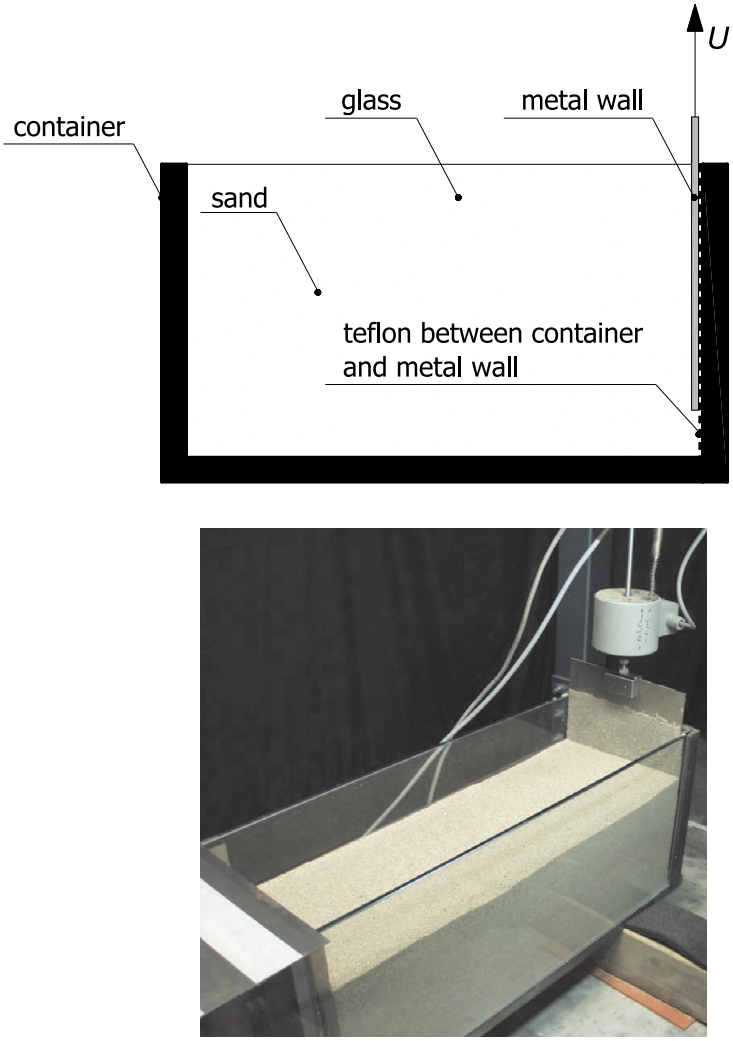

Fig. 5. Experimental set-up for pull-out test

In the experiments, a digital camera Olympus C4040 was used with the image resolution of 2272×1704 pixels. The area of interest (AOI) was 0.15×0.20 m^2. Approximately 30 sand grains were covered by one interrogation cell consisting of a matrix of 16×16 pixels. This satisfied the requirement of a minimum of 5 particles in one cell in order to obtain reliable results (Raffel et al 1998). A separate grain of sand was described approximately with 8 pixels ($16 \times 16 = 256/30 \approx 8$). An adaptive multi-pass process was applied to calculate the displacement field, where the initial cell size of 64×64 pixels was reduced to a fixed smaller cell size of 16×16 pixels (Nübel 2002). A first vector field of the big cell was used as a reference vector field for the next evaluation with a smaller

cell size. A 7 × 7 smoothing filter was used to calculate the displacement field in sand (DaVis PIV Manual 2002). In this case, the differences between the results with the filter and without the filter turned out to be the smallest ones. This filter turned out to be also the most exact to determine the shear zone thickness during a biaxial compression (Kohse 2003).

Fig. 6 shows the load-displacement curves for different initial void ratios e_0. The lower the initial void ratio, the larger the maximum pull-out force. The evolution of the volume strain is demonstrated in Fig. 7 for the different wall roughness in dense sand. The magnitude of strain is expressed by a colour intensity scale attached to the Figure (the maximum volumetric strain is 0.1%). The photographs were made every 0.05 mm with respect to the vertical wall displacement (i.e. every 6 s).

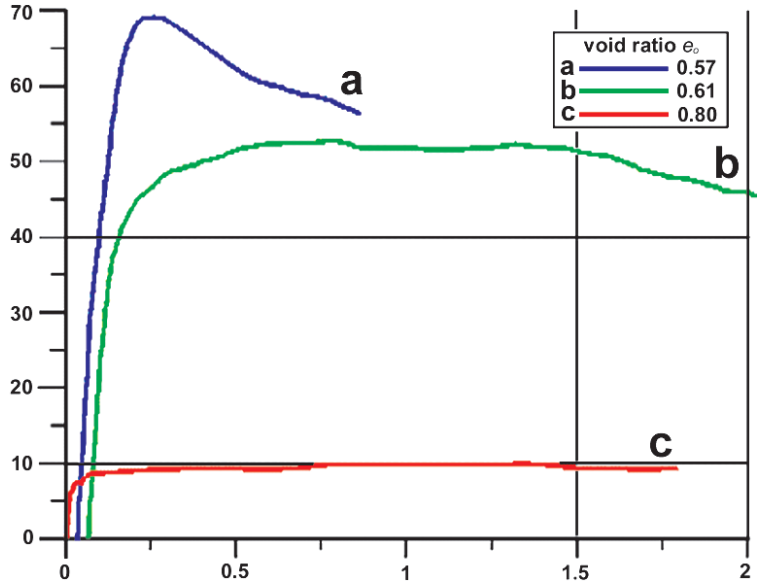

Fig. 6. Load-displacement curve during pull-out test with a very rough wall for different void-ratios e of Karlsruhe sand (P – vertical pull-out force, u – vertical wall displacement)

At the beginning of the pull-out test with the rough and very rough wall, a localized dilatant zone occurs at the wall bottom. It propagates towards the free surface under an angle of about 65°–70° with respect to the bottom. It becomes curvilinear near the upper surface. Afterwards, the whole material between the localized zone and the wall is subjected to strong dilatancy. In the case of smooth wall, a dilatant region behind the wall has a smaller inclination with respect to the bottom (about 45°) and undergoes significantly smaller volume changes. Large volume changes take place only along the wall.

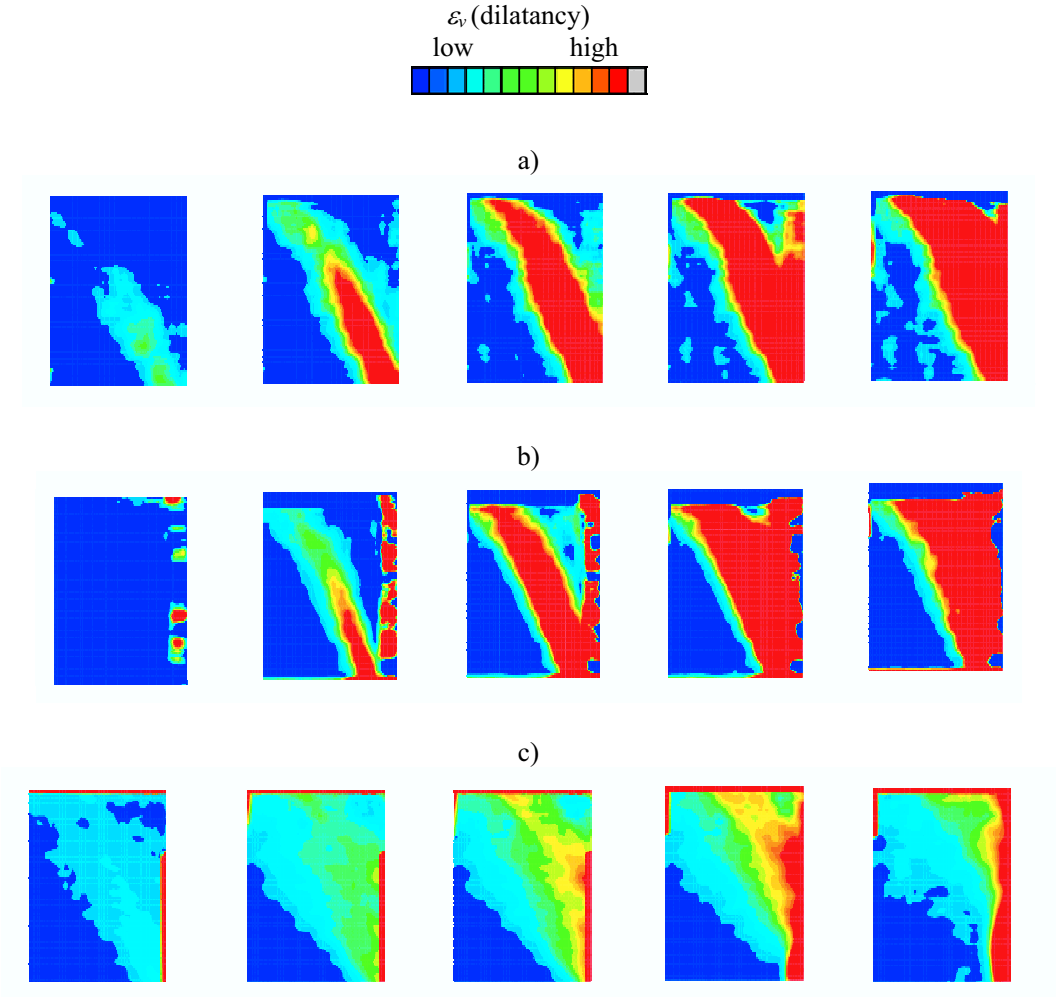

Fig. 7. Evolution of the volume strain ε_v in dense Karlsruhe sand during pull-out test: a) very rough wall, b) rough wall, c) smooth wall

3.2. Dynamic Silo Flow

The experiments were carried out with rectangular perspex symmetric model silos (mass flow silo and funnel flow silo) consisting of a bin and a hopper (Fig. 8). The height of the mass flow silo was $h = 0.32$ m, the width – $b = 0.09$ m, the depth – 0.07 m and the outlet width – 5.0 mm. The height of the funnel flow silo was $h = 0.29$ m, the width – $b = 0.15$ m, the depth – 0.07 m and the outlet width – 5.0 mm. The wall thickness was 0.005 m. The tests were performed with medium dense ($e_0 = 0.70$) and dense ($e_0 = 0.60$) so-called Borowiec sand (mean grain diameter of $d_{50} = 1.0$ mm, uniformity coefficient $U = 5$). Medium dense

sand was obtained by filling the model silo from a feeder hopper fixed above the silo (in the symmetry-axis). In turn, dense sand was obtained by densification of medium dense sand with shocks brought to the silo wall. Silo fill was emptied gravitationally. Smooth and very rough walls in a bin and a hopper were used. A large wall roughness was obtained by gluing a sand paper to the interior wall surfaces. For each case, 4 tests were carried out. All experiments were performed in an air-conditioned room with a temperature of 20°C and relative humidity of 60%.

A Sony DSC P-71 digital camera was used with image resolution of 2560 × 1920 pixels. The area of interest (AOI) was 0.09×0.2 m^2 (mass flow silo) and 0.15×0.2 m^2 (funnel flow silo). Approximately 9 sand grains were covered by one interrogation cell consisting of a matrix of 16×16 pixels. A separate grain of sand was described approximately with 28 pixels ($16 \times 16 = 256/9 \approx 28$). The total emptying time was about 45 s. The photographs were performed precisely at the time interval of $t = 1.0$ s (a further reduction of the time interval was not feasable for technical reasons). The camera was fixed at a distance of $s = 0.4$ m from the fixed silo model with the axis oriented perpendicularly to the plane of deformation. To reduce shadow effect, two 500-watt flashes were used for continuous illumination. No polarization filter was used for the camera. The material was manually released from a silo. The initial experiments have shown that a twice smaller AOI (with $s = 0.20$ m) and a larger time interval ($t = 2.0$ s) insignificantly influenced the results An adaptive multi-pass process and a 7×7 smoothing filter were used (DaVis PIV Manual 2002) to calculate the displacement field in sand.

The results of changes of the volume strain ε_v (from contractancy to dilatancy) and deviatoric strain ε_p in sand during flow in the model silo up to $h = 0.20$ m are shown in Figs. 9–11 (mass flow silo) and Figs. 12–14 (funnel flow silo). The magnitude of the strain change is expressed by the colour intensity scale attached to Figures. The colour scale was always the same. The maximum contractancy and dilatancy were about 0.1% and 0.25%, respectively. The maximum deviatoric strain was 0.1%. All photograhs were converted from an 24-bit image (with 16 milions colours) into 8-bit image with 256 grey shadows.

The results in the silo with smooth walls show that mass flow is non-symmetric and the distribution of density is strongly non-uniform (Fig. 9). The non-uniformity is larger in a medium dense fill. The changes of the deviatoric strain are significantly larger in the bin than in the hopper. In turn, large volume strain changes take place in the entire silo. The largest volume and deviatoric strain changes appear at the transition zone between the bin and hopper. No shear zones were observed along smooth walls.

The material flow in a model silo with very rough walls in the bin and smooth walls in the hopper is also non-symmetric and non-uniform (Fig. 10). The volume and deviatoric strain changes are larger than in a silo with smooth walls. The volume changes (dilatancy) are the largest at the transition zone between the

a)

b)

Fig. 8. Model silo with smooth walls: a) mass flow silo, b) funnel flow silo

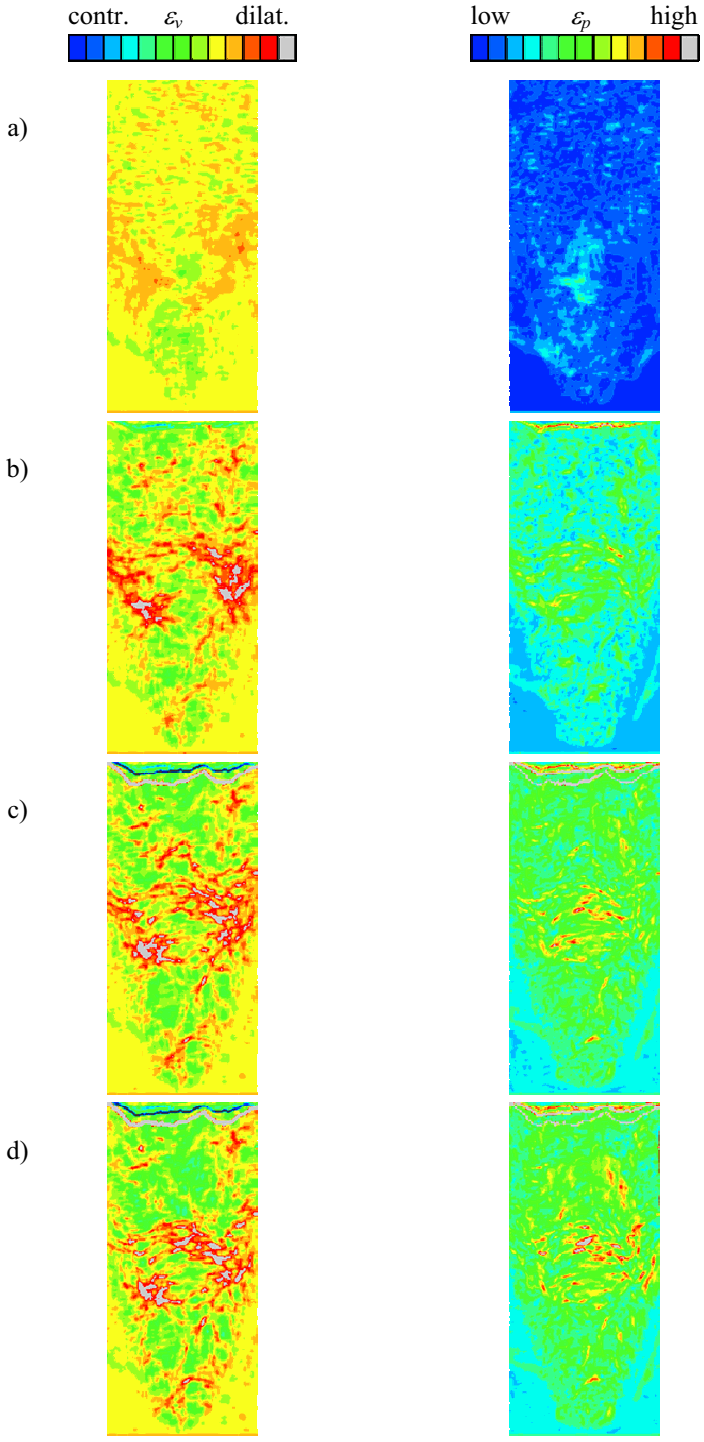

Fig. 9. Evolution of the volume strain ε_v and deviatoric strain ε_p after: a) 1 s, b) 3 s, c) 5 s and d) 7 s of emptying (medium dense Borowiec sand, mass flow silo with smooth walls in bin and smooth walls in hopper)

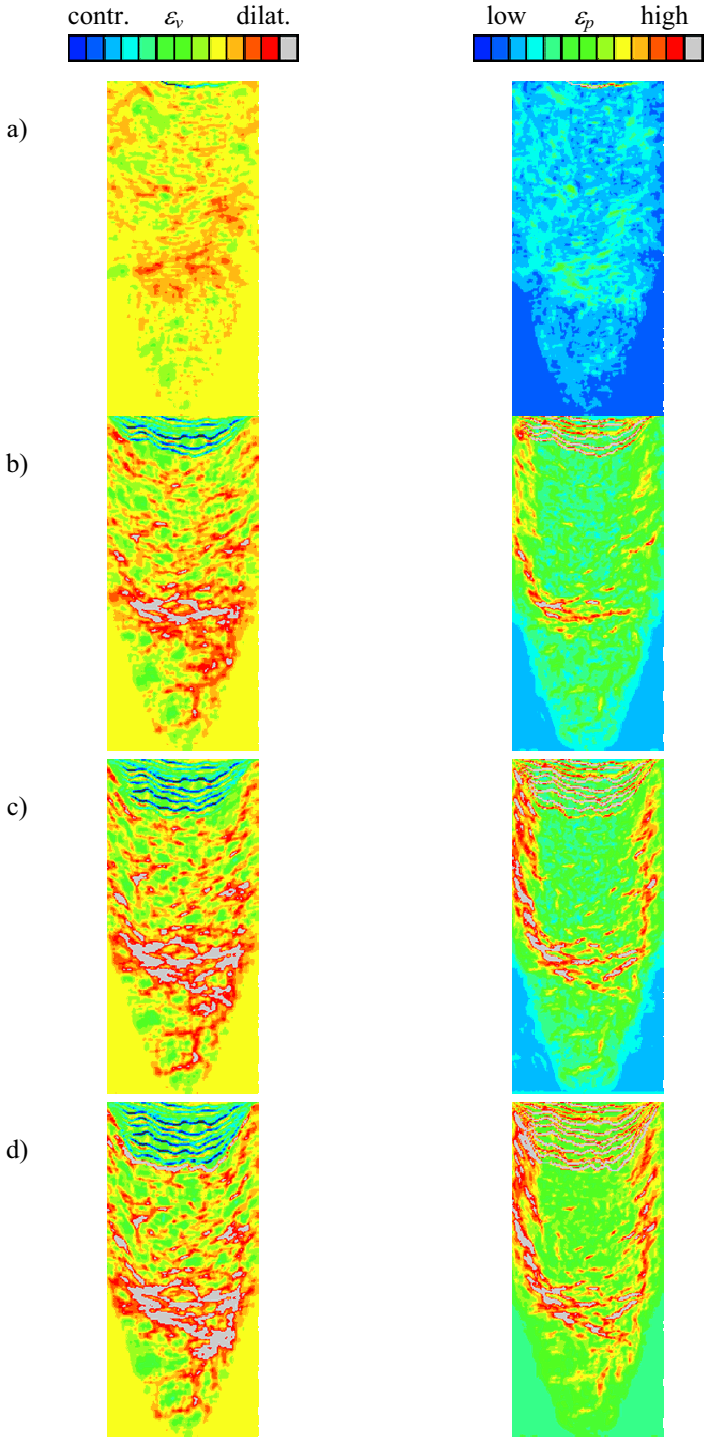

Fig. 10. Evolution of the volume strain ε_v and deviatoric strain ε_p after: a) 1 s, b) 3 s, c) 5 s and d) 7 s of emptying (medium dense Borowiec sand, mass flow silo with very rough walls in bin and smooth walls in hopper)

bin and hopper. Clear shear zones (connected to material dilatancy) are created along the bin walls with a thickness of about 1.5 cm (on the basis of ε_p). These shear zones are similar to those obtained with coloured layers (Tejchman 1989). The distribution of the volume changes in the hopper is similar to that in the silo with smooth walls. The shear dilatant zones spreading between the bin walls are almost horizontal.

In the case of very rough walls in the whole silo, the shear dilatant zones in the bin become parabolic (Fig. 11).

For the funnel flow silo, the distribution of the volume and deviatoric strain is similar irrespective of the wall roughness (Figs. 12–14). The dilatant zones along the material standing motionless at the wall and inside the core are non-symmetric. The shear dilatant zones spreading in the silo between very rough vertical walls can be almost horizontal.

The behaviour of granular materials during granular flow in silos is complex due to the change of the shearing direction at the outlet induced by the hopper form. The material is continuously subject to alternating both local volume changes (from dilatancy to contractancy) and local pressure changes (from increase to release, Tejchman 1997). The behaviour of the material during confined flow in silos can be approximately compared to its behaviour between two states: simple shearing along the wall with constant volume and simple shearing along the wall with constant pressure. During the change of the direction of shearing with constant pressure, material is subject to contractancy after dilatancy. In turn, during the change of the direction of shearing with constant volume, a release of pressure occurs. Flow non-symmetry in silos is caused by an anisotropic character of granular bodies which build discrete systems composed of grains with different shape, size, roundness and roughness.

Radigraphs of silo flow in a mass flow silo with smooth walls (Michalowski 1984, 1990) revealed that a symmetrical pair of curvilinear, dilatant rupture zones was created in the neighborhood of the outlet (Fig. 15a). The zones propagated upward, crossed each other around the symmetry of the silo, reached the walls and subsequently were reflected from them. This process repeated itself until the zones reached the free boundary in the converging hopper or the transition zone in the parallel-converging silo. In the case of a funnel flow silo (Michalowski 1984, 1990, Baxter and Behringer 1990), the curvilinear dilatant zones, in the material core were almost symmetric about a vertical mid-line (Fig. 15b). Some of them propagated upwards or crossed each other.

In our experiments with smooth walls in the entire silo, the distribution of the volume strain in the hopper is only approximately similar to a regular network of arches with low density observed by Michalowski (1984, 1990), and Baxter and Behringer (1990) during mass flow. However, the observed dilatant zones in our tests are much more non-symmetric and non-regular. It is probably caused by the non-uniform distribution of the initial void ratio induced by the filling method

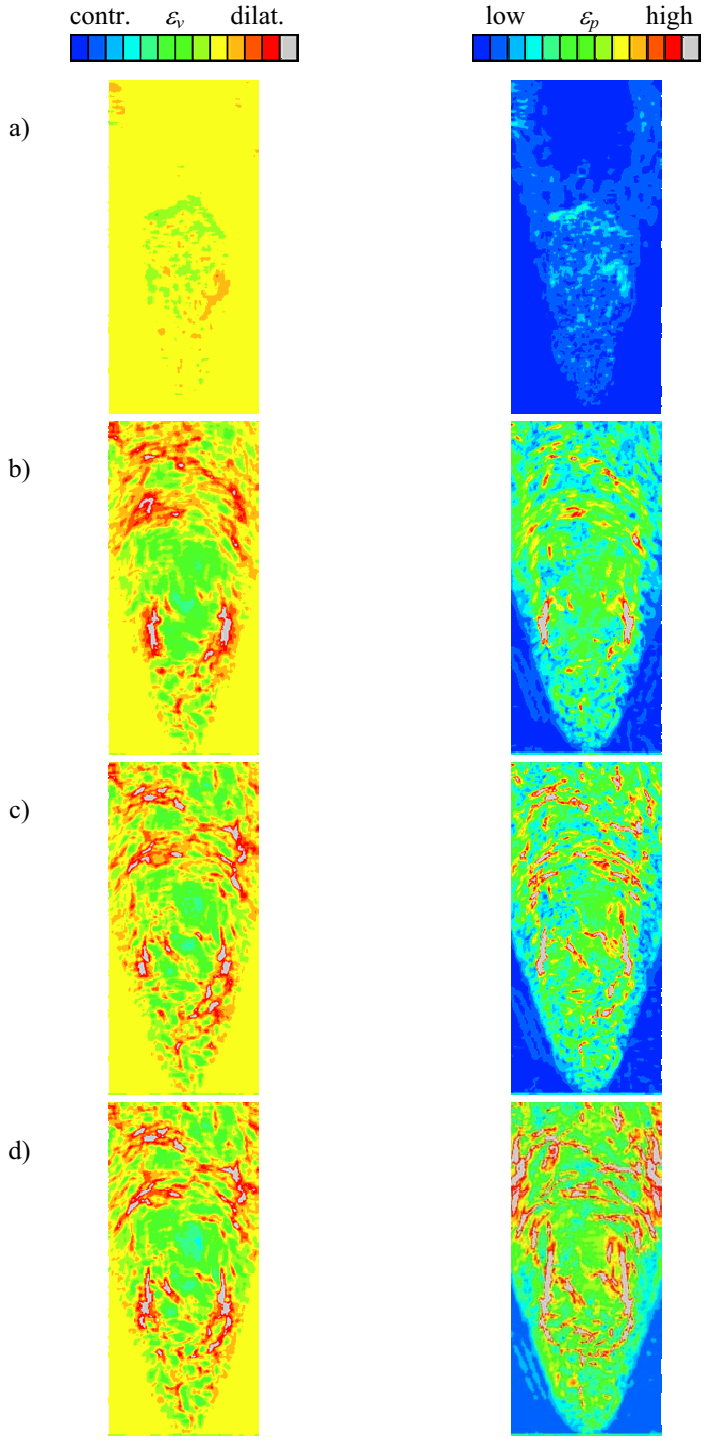

Fig. 11. Evolution of the volume strain ε_v and deviatoric strain ε_p after: a) 1 s, b) 3 s, c) 5 s and d) 7 s of emptying (dense Borowiec sand, mass flow silo with very rough walls in bin and hopper)

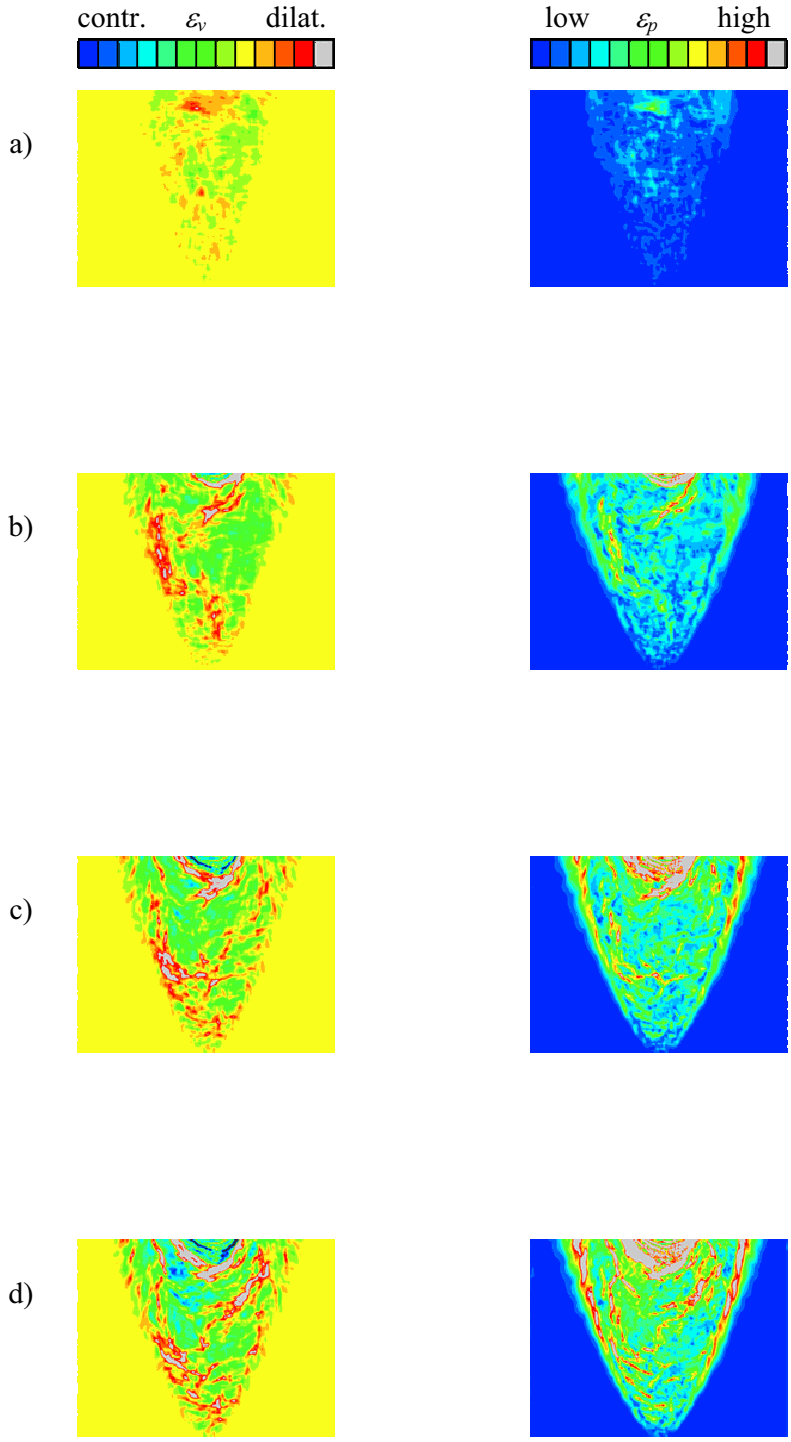

Fig. 12. Evolution of the volume strain ε_v and deviatoric strain ε_p after: a) 1 s, b) 3 s, c) 5 s and d) 7 s of emptying (medium dense Borowiec sand, funnel flow silo with smooth walls in bin and hopper)

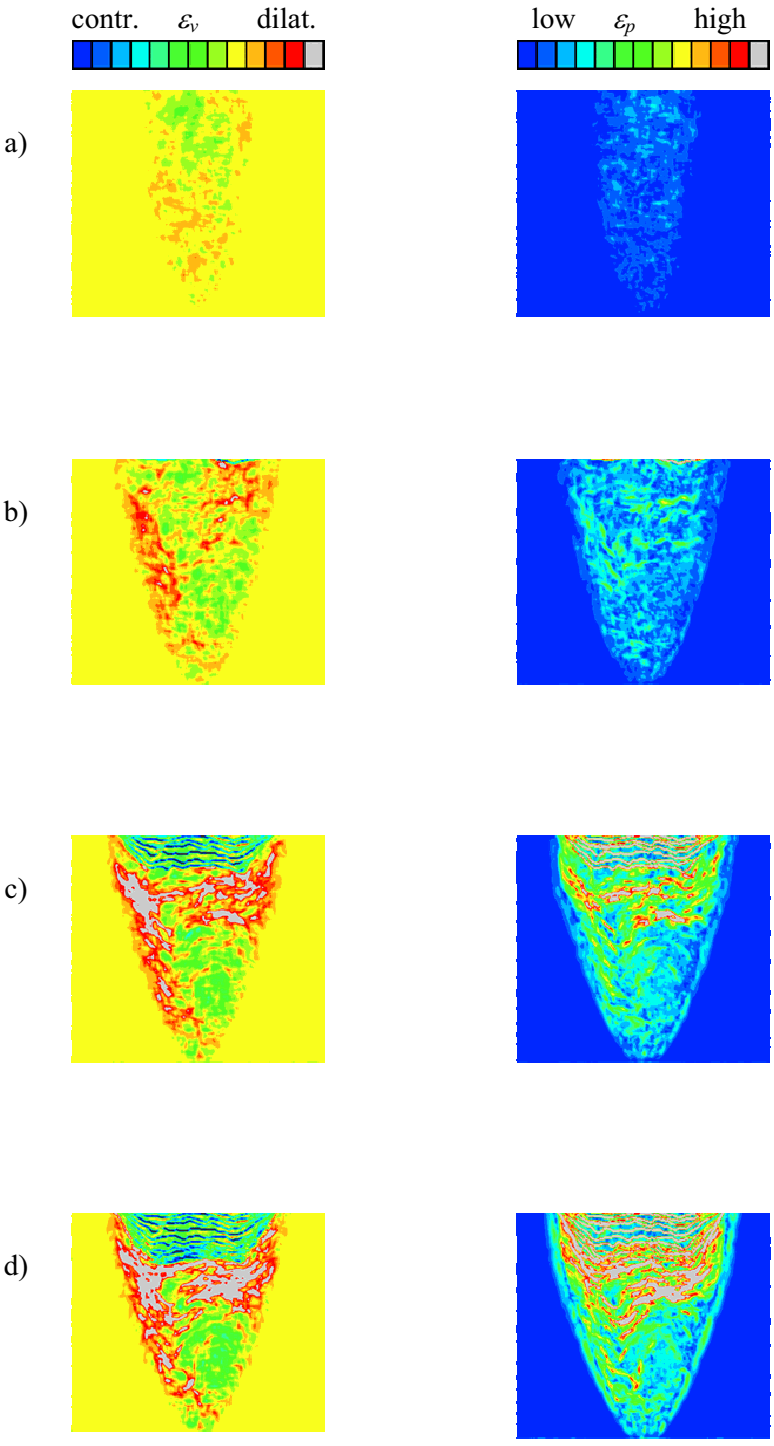

Fig. 13. Evolution of the volume strain ε_v and deviatoric strain ε_p after: a) 1 s, b) 3 s, c) 5 s and d) 7 s of emptying (dense Borowiec sand, funnel flow silo with very rough walls in bin and hopper)

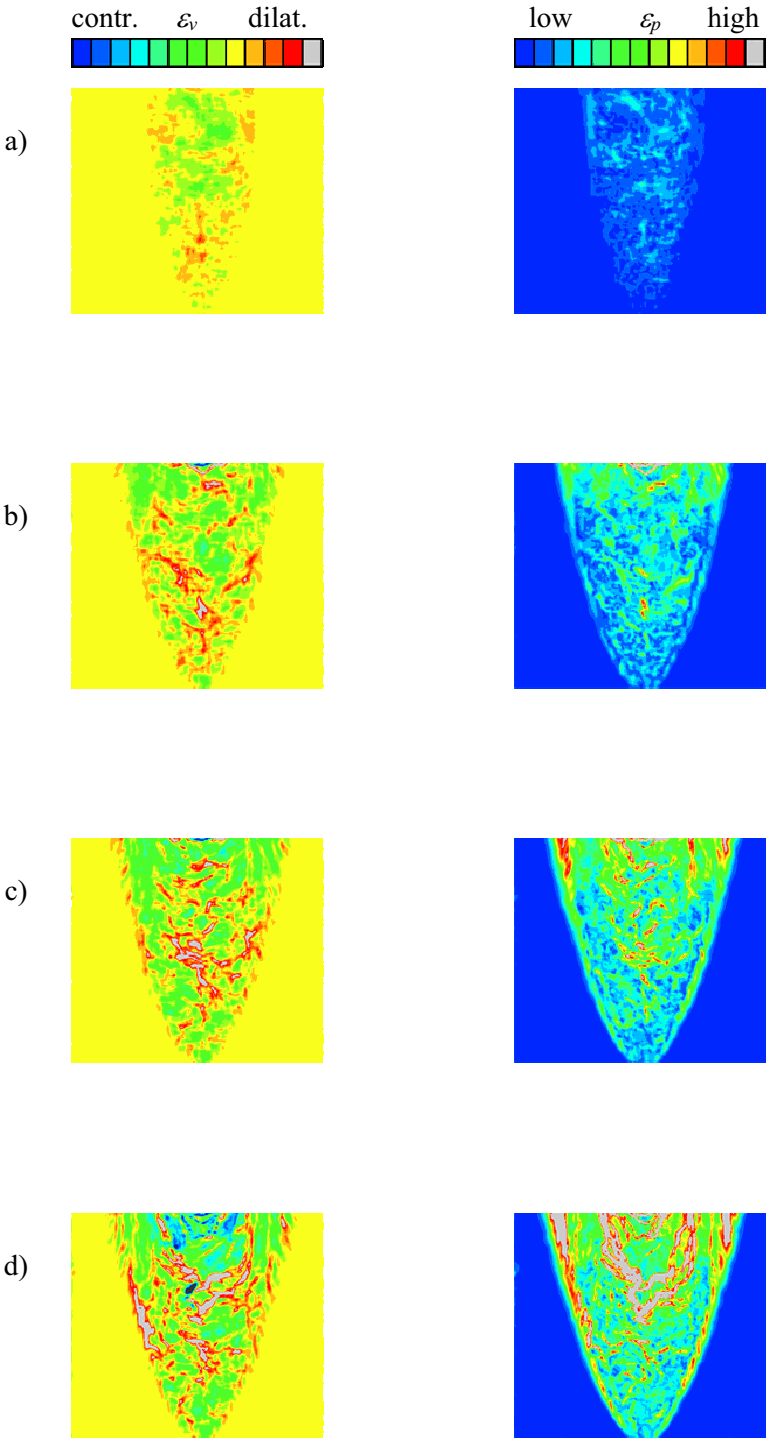

Fig. 14. Evolution of the volume strain ε_v and deviatoric strain ε_p after: a) 1 s, b) 3 s, c) 5 s and d) 7 s of emptying (dense Borowiec sand, funnel flow silo with very rough walls in bin and hopper)

and worse accuracy of X-rays used to measure sand deformations. However, the explanation of these differences requires further investigations.

a)

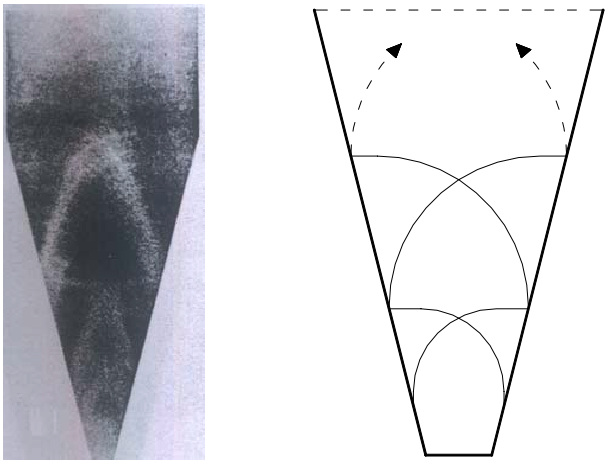

b)

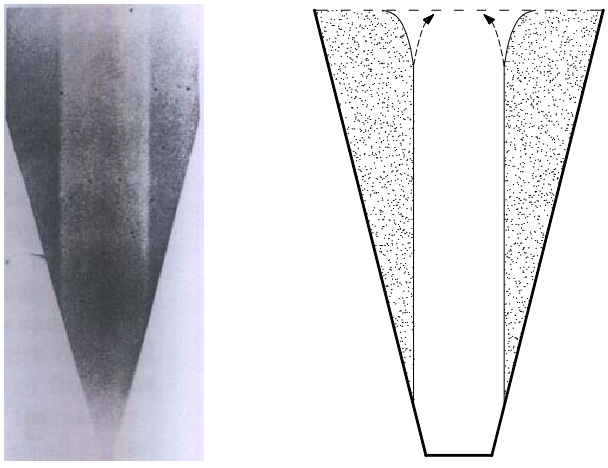

Fig. 15. X-radiographs of (a) mass flow and (b) funnel flow (Michalowski 1984, 1990)

4. Conclusions

Basing on the experimental results presented herein, the following conclusions can be drawn:

- The Particle Image Velocimetry (PIV) method can be used as an effective optical technique to measure deformations in granular materials without any physical contact. This is a highly accurate technique.
- The pull-out tests with rigid wall show that dilatant region occurs in dense sand behind the wall inclined under the angle of 65°–70° with respect of the bottom in the case of a very rough and rough wall and 45° in the case of a smooth wall.
- The experiments during granular silo flow with smooth and rough walls showed that flow is strongly non-symmetric and non-uniform due to the occurrence of dilatant rupture zones. The deformation pattern depends on the wall roughness for mass flow and is independent of the wall roughness for funnel flow. In particular, the volume and deviatoric changes are strongly non-uniform in the hopper, at the transition zone between the bin and the hopper and along very rough bin walls in the case of mass flow. The zones of large deviatoric and volume strains along the bin width can be almost horizontal (bin with very rough walls and hopper with smooth walls) or parabolic (bin and hopper with very rough walls) during mass flow. They can also be horizontal during funnel flow in a silo with very rough walls. Along very rough bin walls, shear localization occurs.
- The experiments with granular flow in silos will be continued. The effect of the filling technique and outflow rate will be carefully studied. The systematic errors and inaccuracies will be precisely estimated. The volume changes will be quantitatively estimated. A CCD-camera with a higher resolution will be used. The experiments with a significantly lower outflow rate will allow us to better determine the displacement field in the silo fill. The test results will be compared with FE-results on the basis of a micro-polar hypoplastic constitutive model (Tejchman 2002, 2004) wherein the stress and couple stress changes are the function of void ratio, pressure level, direction of deformation and mean grain diameter of granulate. The distribution of the initial void ratio will be assumed to be stochastic in FE-calculations (with a spatial correlation, Tejchman 2006).

References

Adrian R. J. (1991), Particle imaging technique for experimental fluid mechanics, *Ann. Rev. Fluid Mech.*, 23, 261–304.

Baxter G. W., Behringer R. P. (1990), *Pattern formation and time-dependence in flowing sand,* [in:] *Two Phase Flows and Waves*, Springer Verlag, New York, 1–29.

Bhandari A. R., Inoue J. (2005), Experimental study of strain rates effects on strain localization characteristics of soft rocks, *Soils and Foundations*, 45, 1, 125–140.

Butterfield R., Harkness R. M., Andrawes K. Z. (1970), A stereo-photogrammetric technique for measuring displacement fields, *Geotechnique*, 20, 3, 308–314.

DaVis PIV Manual (2002), La Vision.

Desrues J. (1984), *La Localization de la Deformation dans les Materiaux Granulaires*, PhD thesis, USMG and INPG, Grenoble.

Desrues J., Chambon R., Mokni M., Mazerolle F. (1996), Void ratio evolution inside shear bands in triaxial sand specimens studied by computed tomography, *Geotechnique,* 46, 3, 529–546.

Desrues J., Viggiani G. (2004), Strain localization in sand: overview of the experiments in Grenoble using stereophotogrammetry, *Int. J. Numer. Anal. Methods in Geomech.,* 28, 4, 279–324.

Fischer R., Gondret P., Rabaud M., Courrech du Pont S., Perrin B. (2005), Velocity fields of intermittent granular avalanches, *Proc. Int. Conf. Powders and Grains 2005* (eds.: R. Garcia-Rojo, H. J. Herrmann and S. McNamara), Taylor and Francis Group, London, 803–805.

Gudehus G. (1986), Einige Beiträge der Bodenmechanik zur Entstehung und Auswirkung von Diskontinuitäten, *Felsbau,* 4, 190–195.

Hutter K., Kirchner N. (2003), *Dynamic Response of Granular and Porous Materials under Large and Catastrophic Deformations*, Springer, New York.

James R. (1965), *Stress and Strain Fields in Sand*, PhD Thesis, University of Cambridge.

Jaworski A., Dyakowski T. (2001), Application of electrical capacitance tomography for measurement of gas-solids flow characteristics in a pneumatic conveying system, *Measurement Science and Technology*, 12, 1109–1119.

Kohse W. C. (2003), *Experimentell Untersuchung von Scherfugenmustern in Granulaten,* Diplomarbeit, Institute for Soil and Rock Mechanics, University of Karlsruhe.

Lueptov R. M., Akonur A., Shinbrot T. (2000), PIV for granular flows, *Experiments in Fluids,* 28, 183–186.

Michalowski R. L. (1984), Flow of granular material through a plane hopper, *Powder Technology*, 39, 29–40.

Michalowski R. L. (1990), Strain localization and periodic fluctuations in granular flow processes from hoppers, *Geotechnique,* 40, 3, 389–403.

Mokni M. (1992), *Relations entre Deformations en Masse et Deformations Localisees dans les Materiaux Granulaires*, PhD thesis, University of Grenoble.

Niedostatkiewicz M., Tejchman J. (2005), Measurements of changes of the bulk solid density during granular flow in silos, *Powder Handling Processing*, Vol. 17, 2, 76–83.

Nübel K. (2002), *Experimental and Numerical Investigation of Shear Localisation in Granular Materials*, Publication Series of the Institute of Soil and Rock Mechanics, University of Karlsruhe, 62.

Raffel M., Willert C., Kompenhaus J. (1998), *Particle Image Velocimetry,* Springer, Berlin, Heidelberg.

Rechenmacher A. L., Finno R. J. (2004), Digital image correlation to evaluate shear banding in dilative sands, *Geotechnical Testing Journal*, 27, 1, 13–22.

Roscoe K. H., Arthur J. R. F., James R. G. (1963), The determination of strains in soils by an X-ray method, *Civ. Eng. Public Works Rev.*, 58, 873–876, 1009–1012.

Sielamowicz I., Kowalewski T. A., Błoński S. (2005), Application of digital particle image velocimetry in registrations of central and eccentric granular material flows, *Proc. Int. Conf. Powder and Grains* (eds. R. Garcia-Rojo, H. J. Herrmann, S. McNamara), 903–908.

Sutton M. A., McNeill S. R., Helm J. D., Chao Y. J. (2000), Advances in two-dimensional and three-dimensional computer vision, *Photemechanics, Topics in Applied Physics*, 77, 323–372.

Tan S., Fwa T. (1991), Influence of voids on density measurements of granular materials using gamma radiation techniques, *Geotech. Test Journal*, 14, 3, 257–265.

Tejchman J. (1989), *Scherzonenbildung und Verspannungseffekte in Granulaten unter Berücksichtigung von Korndrehungen,* Publication Series of the Institute of Soil and Rock Mechanics, University of Karlsruhe, 117, 1–236.

Tejchman J., Wu W. (1995), Experimental and numerical study of sand-steel interfaces, *Int. Journal of Numerical and Anal. Methods in Geomechanics,* 19, 8, 513–537.

Tejchman J. (1997), *Modelling of Shear Localization and Autogeneous Dynamic Effects in Granular Bodies,* Habilitation Monography, University of Karlsruhe, 140, 1–353.

Tejchman J. (2002), Patterns of shear zones in granular bodies within a polar hypoplastic continuum, *Acta Mechanica*, 155, 1–2, 71–95.

Tejchman J. (2004), Influence of a characteristic length on shear zone formation in hypoplasticity with different enhancements, *Computers and Geotechnics*, 31, 8, 595–611.

Tejchman J. (2006), Effect of fluctuation of current void ratio on the shear zone formation in granular bodies within micro-polar hypoplasticity, *Computers and Geotechnics* (in press).

White D. J., Take W. A., Bolton M. D. (2003), Soil deformation measurements using particle image velocimetry (PIV) and photogrammetry, *Geotechnique,* 53, 7, 619–631.

Vacher P., Dumoulin S., Morestin F., Mguil-Touchai S. (1999), Bidimensional strain measurement using digital images, *Proc. Inst. Mech. Eng.*, 213, 811–817, C.

Vardoulakis I. (1977), *Scherfugenbildung in Sandkörpern als Verzweigungsproblem,* PhD thesis, Institute for Soil and Rock Mechanics, University of Karlsruhe, 70.

Yoshida T., Tatsuoka F., Siddique M. (1994), Shear banding in sands observed in plane strain compression, [in:] *Localisation and Bifurcation Theory for Soils and Rocks* (eds.: R. Chambon, J. Desrues and I. Vardoulakis), Balkema, Rotterdam, 165–181.

Zadroga B., Malesiński K. (2005), Novel measurement techniques for subsoil displacements in model tests of the foundation stability, *Inżynieria Morska i Geotechnika*, 3, 208–218 (in Polish).